

This discussion paper is/has been under review for the journal Atmospheric Chemistry and Physics (ACP). Please refer to the corresponding final paper in ACP if available.

Borneo vortex and meso-scale convective rainfall

S. Koseki et al.

Borneo vortex and meso-scale convective rainfall

S. Koseki³, T.-Y. Koh^{1,2}, and C.-K. Teo³

¹School of Physical and Mathematical Science, Nanyang Technological University, Singapore

²Earth Observatory of Singapore, Nanyang Technological University, Singapore

³Temasek Laboratories, Nanyang Technological University, Singapore

Received: 28 May 2013 – Accepted: 31 July 2013 – Published: 13 August 2013

Correspondence to: T.-Y. Koh (kohty@ntu.edu.sg)

Published by Copernicus Publications on behalf of the European Geosciences Union.

Title Page

Abstract

Introduction

Conclusions

References

Tables

Figures

◀

▶

◀

▶

Back

Close

Full Screen / Esc

Printer-friendly Version

Interactive Discussion



Abstract

We have investigated how the Borneo vortex develops over the equatorial South China Sea under cold surge conditions in December during the Asian winter monsoon. Composite analysis using reanalysis and satellite datasets has revealed that absolute vorticity and water vapour are transported by strong cold surges from upstream of the South China Sea to around the equator. Rainfall is correspondingly enhanced over the equatorial South China Sea. A semi-idealized experiment reproduced the Borneo vortex over the equatorial South China Sea during a “perpetual” cold surge. The Borneo vortex is manifested as a meso- α cyclone with a comma-shaped rainband in the northeast sector of the cyclone. Vorticity budget analysis showed that the growth of the meso- α cyclone was achieved mainly by vortex stretching. The comma-shaped rainband consists of clusters of meso- β scale rainfall patches. The warm and wet cyclonic southeasterly flow meets with the cold and dry northeasterly surge forming a confluence front in the northeastern sector of the cyclone. Intense upward motion and heavy rainfall result both due to the low-level convergence and the favourable thermodynamic profile at the confluence front. At both meso- α and meso- β scales, the convergence is ultimately caused by the deviatoric strain in the confluence wind pattern but is much enhanced by nonlinear self-enhancement dynamics.

1 Introduction

Activity of the Asian monsoon is related with the seasonal migration of the Intertropical Convergence Zone (ITCZ; e.g., Hubert et al., 1969) and plays a key role for the climate and weather systems in the Maritime Continent. Basically, the Asian winter monsoon is forced by land-sea thermal contrast between cool Eurasian Continent (at high surface pressure) and warm sea surface in the East and Southeast Asia (at low surface pressure) in boreal winter, e.g., Tomita and Yasunari (1996). Northeasterly winds prevail over the South China Sea (Fig. 2g) in the lower troposphere. This northeasterly

Borneo vortex and meso-scale convective rainfall

S. Koseki et al.

Title Page

Abstract

Introduction

Conclusions

References

Tables

Figures



Back

Close

Full Screen / Esc

Printer-friendly Version

Interactive Discussion



Borneo vortex and meso-scale convective rainfall

S. Koseki et al.

Title Page

Abstract

Introduction

Conclusions

References

Tables

Figures

◀

▶

◀

▶

Back

Close

Full Screen / Esc

Printer-friendly Version

Interactive Discussion



monsoon is cool and dry because the air mass originates on land and the monsoon enhances upward sensible and latent heat fluxes over the South China Sea. The enhanced surface fluxes contribute partly to the generation of the cold tongue in sea surface temperature (SST) (Chen et al., 2003) in the South China Sea during the winter monsoonal season.

Occasionally, the low-level northeasterly winds from the Eurasian Continent associated with the Asian winter monsoon can abruptly intensify. Such rapid intensification of the Asian winter monsoon which is related to the activity of the Siberian High (e.g., Joung and Hitchman, 1982; Takaya and Nakamura, 2005) is commonly known as cold air outbreak or cold surge (although by the time it reaches the Maritime Continent, the air temperature has warmed up considerably due to sensible heat fluxes from the underlying South China Sea). In the mid-latitudes, the cold surge forces the Japan-Sea Polar- Airmass Convergence Zone (JPCZ; e.g., Asai, 1988) and induces the cumulus convection over the Sea of Japan. The cumulus convection brings heavy snowfall around coastal northern Japan (e.g., Nagata, 1987, 1993; Tsuboki and Asai, 2004; Kawashima and Fujiyoshi, 2005). The cold surge induces sudden depression in temperature and increase in sea surface pressure in the coastal Southern China (e.g., Hong et al., 2009; Lu and Chang, 2009). In the Southeast Asia, the cold surge persists for a few days to about one week over the South China Sea and causes severe hazards such as heavy rainfall and flooding (e.g., Wangwongchai et al., 2005; Tangang et al., 2008; Trilaksono et al., 2012). The northeasterly winds can trigger convection by the interaction with local sea/land breeze circulation (e.g., Estoque, 1962) and through the topography lifting effect (e.g., Seko et al., 2008).

Moreover, the cold surge in the Maritime Continent often spins up a meso- α scale cyclonic circulation near Borneo Island, which is sometimes called the Borneo vortex (e.g., Chen et al., 1986; Lau and Chang, 1987; Johnson and Houze, 1987; Juneng and Tangang, 2010; Braesicke et al., 2012). Chang et al. (2005) studied the variability in the Borneo vortex and cold surge using satellite observational and reanalysis datasets. They concluded that the deep cumulus convection tends to occur frequently over the

**Borneo vortex and
meso-scale
convective rainfall**

S. Koseki et al.

Title Page

Abstract

Introduction

Conclusions

References

Tables

Figures

◀

▶

◀

▶

Back

Close

Full Screen / Esc

Printer-friendly Version

Interactive Discussion



South China Sea in the presence of the Borneo vortex. The Borneo vortex generally has a shallow vertical structure, but in the extreme case, it could grow to become a tropical storm, and in one instance, even a typhoon with a deep vortex tube and a well-formed eyewall despite the proximity to the equator. This singular event is the typhoon Vamei which formed over the equatorial South China Sea (around 1.5° N) on 26 December, 2001 (e.g., Chang et al. 2003; Chambers and Li, 2007). Chang et al. (2003) indicated that the persistence of the cold surge over the South China Sea and the quasi-stationary location of the Borneo vortex over the sea for more than one week was necessary for this exceptional case of tropical cyclogenesis. Chambers and Li (2007) ran a model simulation and diagnosed that rapid development in potential vorticity is responsible for the typhoon generation.

While tropical cyclogenesis rarely occurs, the formation of heavily precipitating meso- β convective systems in the presence of Borneo vortex is a common occurrence and brings heavy rainfall to the surrounding coastal regions during the winter monsoon. There is room for more research to understand the formation and the organization of clusters of these smaller but more frequent systems. While Chen et al. (2012a) showed that the interannual variation in rainfall in the region is related with the synoptic-scale cyclonic disturbances over and around the South China Sea, the mechanisms through which mesoscale convective systems are caused by the disturbances has not been clarified. Given that there are few diagnostic or dynamical analyses on such topics, we shall explore the mechanism of generation and organization of deep convection through the development of Borneo vortex over equatorial South China Sea.

This paper is divided into two parts: the first focuses on composite data analysis, in which we investigate the difference in synoptic-scale atmospheric fields between the climatology and cold surge cases and reveal the dynamical relationship between the cold surge and Borneo vortex; the second involves a numerical experiment using a nonhydrostatic model in order to examine how the deep cumulus convection is formed in the presence of the Borneo vortex and cold surge, which is not captured by the low resolution datasets in this region. Because we attempt to investigate the general case

of the Borneo vortex, we conduct the numerical experiment not for a certain event, but for semi-idealized conditions.

In Sect. 2, we describe the details of the datasets and model used in this study. We present results of data analysis for the cold surge and the associated Borneo vortex in Sects. 3 and 4. We show the results of the numerical experiment in Sect. 5. In Sect. 6, we synthesize and discuss the results of Sects. 3, 4 and 5. Finally, concluding remarks are made in Sect. 7.

2 Data and numerical model

For investigation of synoptic-scale atmospheric features associated with the cold surge, we use daily Japanese 25-year Reanalysis (JRA25, Onogi et al., 2007) and Japanese Meteorological Agency (JMA) Climate Data Assimilation System (JCDAS) dataset with $1.25^\circ \times 1.25^\circ$ horizontal resolution and 23 vertical layers of p coordinate in December from 1981 to 2008 (JRA25 is from 1981 to 2004 and JCDAS is from 2005 to 2008 because of modulation in the operational system). Also, we use 3hourly rainfall data in December from 1998 to 2008 obtained from Tropical Rainfall Measurement Mission (TRMM) version 3B42 dataset with horizontal resolution of $0.25^\circ \times 0.25^\circ$ (Huffman et al., 2007).

To conduct the numerical experiments, the Non-Hydrostatic Model version.2010-May-10 (NHM, Saito et al., 2006; Saito et al., 2007) developed by JMA is used in our study. NHM is an operational weather forecasting model suitable to resolve meso-scale phenomena. Hayashi et al. (2008) evaluated NHM simulations of rainfall in Maritime Continent on weather time scales.

In this study, horizontal and vertical resolutions of NHM are set to be 10 km and 40 vertical layers (with the model top at 22 055 m using a terrain following coordinate; 34 levels in the troposphere including 9 levels in the first km). We select the Kain-Fritsch cumulus scheme (Kain, 2004), the 6-class cloud microphysics (Ikawa and Saito, 1991), the improved Mellor-Yamada level-3 turbulent closure scheme (Nakanishi, 2001;

Borneo vortex and meso-scale convective rainfall

S. Koseki et al.

Title Page

Abstract

Introduction

Conclusions

References

Tables

Figures



Back

Close

Full Screen / Esc

Printer-friendly Version

Interactive Discussion



Nakanishi and Niino, 2004 and 2006), and the 4-layer land surface scheme (Kumagai, 2004a). Topography and land use data are obtained from Global 30 Arc Second Elevation Data Set (GTOPO30) and Global Land Cover Characterization (GLCC) of United States Geological Survey (USGS). Other detailed setting such as boundary and initial conditions of numerical model will be given in Sect. 5.

3 Composite analysis of cold surge events

In this section, we examine a composite analysis of observed atmospheric fields, based on strong and no cold surge situations over the South China Sea using JRA25/JCDAS reanalyses and TRMM rainfall data.

3.1 Synoptic-scale atmospheric circulation

For classification of strong and no cold surge cases, we compute Cold Surge (CS) Index (Chang et al., 2005) defined as the area-averaged wind speed at 850 hPa in the box-domain 7.5° N to 12.5° N and 110° E to 115° E. Figure 1 shows the daily December CS Index from 1981 to 2008 obtained from JRA25 and JCDAS. In this study, we define CS Index larger (smaller) than the climatology plus (minus) one standard deviation of CS Index as a strong (no) surge case abbreviated henceforth by SS (NS). SS are seen in almost every year. They occasionally persist for one week or longer, e.g., in 1984, 1990, 1993, 1998, 1999, 2001, 2005, and 2006. It is well-known that strong wind in 2001 helped cause the formation of tropical typhoon Vamei (Chang et al., 2003) at the record-low latitude of 1.5° N. In addition, tropical storm Gil (<http://www.weather.gov.hk/publica/tc/tc1998.pdf>) occurred after SS over the South China Sea between 9 and 12 of December in 1998 estimated from JMA the Regional Specialized Meteorological Centre (RSMC) Tokyo Best track (http://www.jma.go.jp/jma/jma-eng/jma-centre/rsmc-hp-pub-eg/RSMC_HP.htm). CS Index for

Borneo vortex and meso-scale convective rainfall

S. Koseki et al.

Title Page

Abstract

Introduction

Conclusions

References

Tables

Figures

⏪

⏩

◀

▶

Back

Close

Full Screen / Esc

Printer-friendly Version

Interactive Discussion



January has been also examined from 1981 to 2008 (not shown) with similar occurrences of SS and NS albeit under different climatological wind.

Note that we exclude from our study those days of SS associated with the two extreme cases of Vamei (20–24 December, 2001) and Gil (5–8 December, 1998). The reason is to focus on the typical cases of meso-scale circulation and convection associated with strong cold surges, and not be biased by the rare extreme events which may involve atypical tropical cyclogenetic dynamics. Thus, the composite duration of SS and NS amounts respectively to 133 and 156 days in December from 1981 to 2008, i.e. 15% and 18% of the time. In the climatology shown in Fig. 2b, the northeasterly winter monsoon prevails over the South China Sea and when it reaches the Java Sea, it switches direction to northwesterly due to the change in the direction of Coriolis force across the equator. During SS (NS), Fig. 2c (Fig. 2a) shows that the winter monsoon is reinforced (weakened) over the South China Sea and to a lesser extent in the Java Sea. The climatology in Fig. 2e shows that strongly positive absolute vorticity extends from the west of Luzon Island of the Philippines over the South China Sea toward the equator. During SS (NS), Fig. 2f (Fig. 2d) shows that positive (negative) difference in absolute vorticity is found over the South China Sea off the northwestern coast of Borneo and between Sumatra and Borneo; conversely, negative (positive) difference is detected around Indochina. The distribution of the difference in absolute vorticity is approximately opposite during NS and SS. The ratio of the difference in absolute vorticity to climatology of absolute vorticity is about 30% in both SS and NS off the northwestern coast of Borneo.

3.2 Synoptic-scale atmospheric transport

The isobaric divergence of absolute vorticity flux is investigated next, which is defined as $\nabla_p \cdot (\mathbf{V} \zeta_a)$, where \mathbf{V} is horizontal wind vector (u, v), ζ_a is the cross-isobaric component of absolute vorticity, and ∇_p is the isobaric gradient operator. Large convergence of absolute vorticity flux is located over the South China Sea east of Indochina and Malay Peninsula during SS (Fig. 3a). Equally strong divergence is found further north

Borneo vortex and meso-scale convective rainfall

S. Koseki et al.

Title Page

Abstract

Introduction

Conclusions

References

Tables

Figures



Back

Close

Full Screen / Esc

Printer-friendly Version

Interactive Discussion



**Borneo vortex and
meso-scale
convective rainfall**

S. Koseki et al.

Title Page

Abstract

Introduction

Conclusions

References

Tables

Figures

◀

▶

◀

▶

Back

Close

Full Screen / Esc

Printer-friendly Version

Interactive Discussion



in the west of Luzon Island. This shows that as the winter monsoon blows from north-east to southwest (Fig. 2c), high absolute vorticity is transported southwestward from the northern tropical latitudes toward the equator. In particular, the convergence around the equatorial South China Sea extends to the northwestern coast of Borneo due to the enhanced vorticity transport. At lower levels such as 925 hPa, this patch of flux convergence further extends northeastward along the Borneo coast to around (115° E, 6° N). Averaged between 0° N and 4° N, the flux convergence is largest during SS over the equatorial South China Sea between 100° E and 110° E (Fig. 3c) and the convergence concentrates in the lower troposphere (~ 700 hPa or larger). The positive tendency due to enhanced transport by the winter monsoon during SS favours the generation of Borneo vortex over the equatorial South China Sea.

The isobaric divergence of water vapour flux at 1000 hPa during SS, defined as $\nabla_p \cdot (\mathbf{V}q)$ where q denotes specific humidity, is similar to that of absolute vorticity flux (Fig. 3b): there is equatorward transport of water vapour by the northeast monsoon and similar intensification during SS. Note that the Clausius-Clapeyron relation confines specific humidity and hence its transport mostly below 800 hPa (Fig. 3d). The large convergence during SS suggests that water vapour is concentrated over the equatorial South China Sea by strong cold surges thereby increasing the supply of water for precipitation.

The enhanced equatorward flux of water vapour also sustains the boundary-layer moist static energy for the release of latent heat through convection. The distribution of moist static energy flux divergence matches approximately with that of water vapour flux divergence. Therefore, we can expect convection and rainfall to be much enhanced during SS.

3.3 Rainfall and its diurnal cycle

Rainfall is dominant along the eastern coast of Malay Peninsula, northwestern coast of Borneo, and over the central South China Sea (Fig. 4). This coincides roughly with

that of water vapour flux convergence at 1000 hPa (Fig. 3b) showing the predominant influence of water vapour transport over local evaporation on rainfall in December.

Rainfall in the Maritime Continent has a strong diurnal cycle being brought about by sea/land breeze circulation (e.g., Mak and Walsh, 1976; Hadi et al., 2002; Joseph et al., 2008). Rainfall in the South China Sea manifests a diurnal cycle, but the amplitude of variation is small especially near the equator (Fig. 5a–b). This may be because in the open sea, both the local SST diurnal fluctuation and the effect of land breeze from coastlines are relatively small. During SS (NS) the rainfall is almost uniformly enhanced (reduced) throughout the whole day in the equatorial South China Sea. In contrast, the rainfall over the Java Sea has a large diurnal cycle in the climatology and during SS (NS) it is enhanced (reduced) the most in the morning around 03:00–12:00 LST (06:00–09:00 LST), when the rainfall is maximal (Fig. 5c).

Over the Java Sea, the changes in the diurnal cycle under changing ambient wind is similar to results reported in Qian et al. (2010) and Koseki et al. (2013). When the cold surge is strong, it crosses the equator and reaches Java (Hattori et al., 2011). Because the cold surge comprises northerly wind, the southerly land breeze during the night-morning time from the northern coast of Java tends to generate strong convergence over the Java Sea. This convergence induces low-level rising motion and facilitates the release of potential instability by cumulus convection and rainfall. Our composite analysis has shown that the northerly is stronger (weaker) over the Java Sea during SS (NS) than that in the climatology (Fig. 2a–c) in support of the above mechanism. Moreover, the cold surge contains much water vapour and enhanced convergence of water vapour flux at 850 hPa is detected over the Java Sea during SS (not shown), sustaining the enhancement of the rainfall.

4 Borneo Vortex in JRA25 and JCDAS data

Since during SS the rainfall is intensified the most over the South China Sea near to where the absolute vorticity flux convergence is the strongest, a physical relationship

Borneo vortex and meso-scale convective rainfall

S. Koseki et al.

Title Page

Abstract

Introduction

Conclusions

References

Tables

Figures

◀

▶

◀

▶

Back

Close

Full Screen / Esc

Printer-friendly Version

Interactive Discussion



may exist between absolute vorticity and rainfall activity. In particular, we are interested in those times when the high absolute vorticity manifests as a strong Borneo vortex.

5 Firstly, we define the Marine Borneo Vortex (MBV) Index as the absolute vorticity at 850 hPa averaged over 0° N to 4° N and 105° E to 110° E, which covers the equatorial South China Sea between Malay Peninsula and Borneo. MBV Index tends to be strong when CS Index is also strong (Fig. 6) and vice versa. The correlation coefficient between CS and MBV Indices are 0.35 in December and 0.49 in January, both of which are statistically significant at the 95 % confidence level. This suggests that strong cold surge which transports high absolute vorticity from the north tends to spin up a strong Borneo Vortex in equatorial South China Sea. This idea is supported by the dynamical experiments of Lim and Chang (1981).

10 Next, a strong cold surge event and a strong marine Borneo vortex event are defined as continuous period of elevated daily mean value of CS and MBV Indices respectively, where “elevated” refers to larger than one standard deviation from the climatological mean. A strong cold surge is said to spin up a strong Borneo vortex in the equatorial South China Sea only if two events overlap in time and the former starts at the same time or earlier than the latter. In this way, 58 out of the 133 days of SS are related directly to the strengthening of the Borneo vortex in the equatorial South China Sea. For three of these days, the Borneo vortex is located north of 5° N and takes on a more elongated shape, which is rather exceptional. So subsequent composite analyses use only the other 55 days of data.

20 Figure 7a shows that the strong Borneo vortices during SS occur mostly around the west of Borneo near the equator between 5° N and 2° S where tropical cyclones do not develop (except for the singular case of Typhoon Vamei). This distribution is quite similar to that shown by Chang et al. (2003), although they identified Borneo vortices without regard to the strength of the cold surge. Figure 7b shows that the wind field is not axisymmetric in the composite Borneo vortex with strong northeasterlies in the northeast sector, which is attributed to the strong cold surge. The maximum of absolute vorticity is located slightly northwest from the centre and the ridge of high absolute

Borneo vortex and meso-scale convective rainfall

S. Koseki et al.

Title Page

Abstract

Introduction

Conclusions

References

Tables

Figures



Back

Close

Full Screen / Esc

Printer-friendly Version

Interactive Discussion



vorticity extends northeastward and, to much lesser extent, westward and southeastward. Strong convergence is found in the southern, western and northeastern sectors (Fig. 7c) where strong wind prevails (Fig. 7b). On the other hand, weak divergence is located southeast of the composite vortex overlapping with a patch of weakly negative absolute vorticity. The pattern of intense rainfall is approximately consistent with the pattern of strong convergence with a slight northeastward displacement of the former from the latter.

As JRA/JCDAS data have low resolution and vortices of different sizes and shapes are composited in Fig. 7b and c, it is hard to discern any clear relation between absolute vorticity, wind convergence and rainfall in a Borneo vortex from the above results.

5 Semi-idealized experiment for the Borneo vortex

Based on CS and MBV indices, when the cold surge is strong, the strong Borneo vortex occurs with probability of 44 % (= 58 days/133 days). In this section, to investigate how the rainfall is organized by the strong cold surge and Borneo vortex, we conduct a numerical experiment using NHM (cf. Sect. 2).

5.1 Experimental design

To recreate the synoptic conditions under which the Borneo vortex forms over the equatorial South China Sea numerically, we use the composite data fields of SS shown in the previous section as boundary and initial conditions. Because there is anomalous convergence of the composite absolute vorticity flux over the equatorial South China Sea (Fig. 3a), this situation can be regarded as idealized initial and boundary conditions for generating the Borneo vortex. By holding such lateral boundary conditions constant, the strong cold surge persists and keeps supplying the absolute vorticity, water vapour and moist static energy over the equatorial South China Sea. The integration period is 11 days and we set an expedient initialization date-time of 15 December, 00:00

Borneo vortex and meso-scale convective rainfall

S. Koseki et al.

Title Page

Abstract

Introduction

Conclusions

References

Tables

Figures

◀

▶

◀

▶

Back

Close

Full Screen / Esc

Printer-friendly Version

Interactive Discussion



UTC for the model's diurnally and seasonally dependent radiation scheme. The model spins up effectively within the first day of integration. Horizontal and vertical resolutions are 10 km × 10 km at the equator using Mercator projection and 40 layers in terrain-following coordinate. The centre of domain is at (110° E, 2.5° N) and with 300 × 300 grid points (Fig. 8a). Realistic land-sea mask and terrain height are used. Henceforth, we call this experiment the semi-idealized experiment. We checked that there was no systematic trend in total mass within the domain despite the prescription of boundary winds.

5.2 Simulated Borneo vortex

Figure 8b–k shows the formation and westward movement of the vortex over the equatorial South China Sea in the semi-idealized experiment. In 24 h, meridional wind at 850 hPa is almost southward over the equatorial South China Sea and the Borneo vortex has barely formed yet. Between 48 and 72 hour, weak northward meridional wind is detected around 108° E to 109° E and 1.5° S to 0° N and cyclonic circulation is generated around the equator over the sea. This cyclonic circulation is intensified in 96 h. At this stage, the cyclonic circulation resembles the typical Borneo vortex and the vortex is quasi-stationary. In 120 h, the vortex strength is enhanced more significantly. From 144 to 192 h, the Borneo vortex moves slowly northwestward. This well-developed vortex has a spatial scale between a few hundred to a thousand kilometers, i.e. at the meso- α scale. This meso- α cyclone is unlike a tropical cyclone which is larger, more intense and has distinct dynamics. Between 216 and 240 h, the cyclone reaches over the Malay Peninsula and weakens. Figure 10 illustrates the 24-hourly track of the cyclone centre (defined in Appendix A) from 24 to 240 h.

Figure 9a and b illustrate time sequences of area-averaged absolute vorticity at 850 hPa and hourly rainfall within 200 km from the cyclone centre. The absolute vorticity is less than 10^{-4} s^{-1} until 50 h and becomes gradually intensified until around 140 h. After that, the cyclone, more or less saturates. From 190 h, it weakens rapidly and remains as a weak vortex from 223 h. Rainfall shows a clear diurnal cycle and the

diurnal peak rainfall intensity appears to follow the trend of the absolute vorticity of the meso- α cyclone. Based on these temporal sequences of the cyclone, we can divide the lifecycle of the cyclone into three stages; developing stage (50 to 140 h), mature stage (141 to 190 h), and decaying stage (191 to 223 h).

Figure 10 shows the horizontal distribution of temporal mean of hourly-accumulated rainfall around the cyclone centre at each stage. In the developing stage, rainfall is dominant just west of the cyclone centre and extends northward to ~ 150 km. In the mature stage, the rainfall adjacent to the cyclone centre becomes more intense and a well-developed comma-shaped rainband extends from the centre northward, northeastward and then eastward to reach a distance of 250 km from the centre. This comma-shaped rainband is located only in the northern part of the cyclone and its localization is discussed in Sect. 6. In the decaying stage, the rainfall around the centre is reduced significantly and the distribution is relatively widespread but still mostly in the northern part of the cyclone. Throughout the three stages, no “eye” formation occurs in the cyclone unlike typhoons which form in higher tropical latitudes.

Compared with the composite of the Borneo vortex in TRMM dataset (Fig. 7c), the rainfall is much more localized in the northern and northeastern sector, and one order of magnitude more intense in our semi-idealized experiment. This is expected from the higher resolution of the model which is able to capture the meso- β scale dynamics while TRMM rainfall estimates could be too low due to interfering thick and widespread clouds in the Borneo vortex during data retrieval. Note despite the relative weakness of rain in the southern sector in the numerical simulation (Fig. 10) unlike the relatively intense patch seen there in the composite Borneo vortex (Fig. 7c), the magnitude of the rainfall are actually similar. This southern patch of rain is likely the result of convection at land-breeze fronts propagating northward from Java Island to Java Sea (Koseki et al., 2013) where clouds are patchy and so is well-captured by TRMM data retrievals.

Borneo vortex and meso-scale convective rainfall

S. Koseki et al.

Title Page

Abstract

Introduction

Conclusions

References

Tables

Figures

◀

▶

◀

▶

Back

Close

Full Screen / Esc

Printer-friendly Version

Interactive Discussion



5.3 Vertical structure of the meso- α cyclone

We explore the axisymmetric vertical structure of the meso- α cyclone by averaging the atmospheric variables at equal distances from the cyclonic centre in the mature stage, when the cyclone is most intense. Figure 11a and b illustrate the axisymmetric tangential and radial winds. Tangential velocities beyond 24 m s^{-1} are seen just within 50 km-radius, which is comparable with that of a typical typhoon over the tropical Pacific Ocean (Frank, 1977). However, such strong winds are limited to the lower troposphere (below $\sim 750 \text{ hPa}$) and the tangential wind is weak in the upper troposphere (above $\sim 200 \text{ hPa}$). Thus, the meso- α cyclone in our experiment is shallow, while a typical typhoon has a deeper structure (Frank, 1977). There is radial inflow mainly below $\sim 900 \text{ hPa}$ and radial outflow mainly above radial $\sim 300 \text{ hPa}$. The distribution and magnitude of radial wind are similar to those of typical tropical typhoon over the Pacific Ocean (Holland and Merrill, 1984). The wind speeds are much stronger and the spatial scale is much smaller in our simulation than in the composite Borneo vortex from JRA25/JCDAS (not shown), probably because the global model on which JRA25/JCDAS is based lacks the resolution to support the downscale cascade of kinetic energy in the mesoscale which serve to strengthen and tighten the vortex.

Figure 11c shows the axisymmetric component of mixing ratio of cloud liquid water plus cloud ice (shaded) and vertical velocity (contour) around the cyclone centre in the mature stage. One maximum of cloud water is detected between 900 and 500 hPa around the radius of 50 km. This maximum of cloud water is associated with the deep convection and heavy rainfall adjacent to the cyclone centre (Fig. 10b). The location of the maximum of vertical velocity is roughly consistent with that of cloud water, especially after making allowance for possible outward displacement of hydrometeors due to centrifugal forces in the cyclonic circulation. This strong upward motion is the result of latent heat release by the intense convection around the cyclone centre and drives the radial wind circulation by mass continuity. While the axisymmetric vertical velocity shows negative values (upward), weak non-axisymmetric positive vertical velocity

Borneo vortex and meso-scale convective rainfall

S. Koseki et al.

Title Page

Abstract

Introduction

Conclusions

References

Tables

Figures



Back

Close

Full Screen / Esc

Printer-friendly Version

Interactive Discussion



Borneo vortex and meso-scale convective rainfall

S. Koseki et al.

Title Page

Abstract

Introduction

Conclusions

References

Tables

Figures

◀

▶

◀

▶

Back

Close

Full Screen / Esc

Printer-friendly Version

Interactive Discussion

(downward) can be detected around the centre as part of the local organization of convective downdrafts (not shown). The other maximum of cloud water (mostly in the ice phase) is seen between 300 and 100 hPa and has a large radial extent from 100 km to 350 km. This is because the radial wind at this level is centrifugal and the cloud ice is advected outward. Thus, this cloud cluster can be categorized as the anvils associated with cumulus convection. Moreover, the cloud liquid water and ice do not distribute uniformly around the cyclone centre, but concentrates in the north and northeastern part of the meso- α cyclone (not shown), not unlike the comma-shaped rainband (Fig. 10b).

Figure 11d illustrates the axisymmetric component of temperature (contour) and temperature deviation from the horizontal mean (shaded). Large positive temperature anomaly is found between 900 and 300 hPa within 50 km from the cyclone centre. This is due to the latent heat release by convection near the cyclone centre, and provides positive buoyancy for the rising air at the cyclone centre. This warm core around the centre is also detected by Braesicke et al. (2012). Moreover, the depression in sea level pressure (SLP) at the cyclone centre corresponds well to the positive temperature anomaly aloft as is expected from hydrostatic balance (Fig. 11e). The mesoscale simulation indicates that the central depression could be as much as 13 hPa lower than the ambient SLP, which is an order of magnitude greater than what is recorded in the JRA25/JCDAS dataset at synoptic scale (not shown). This is reasonable because most of the pressure drop occurs within 150 km from the cyclone centre, which is below the limit of the resolution of the JRA25/JCDAS dataset.

6 Analysis and discussion of the numerical experiment

6.1 Growth and maintenance of the meso- α cyclone

To investigate what mechanism leads to the growth of the meso- α scale cyclone, we examine the absolute vorticity dynamics in this subsection.

Appendix B shows that in the reference frame co-moving with the cyclone centre, the tendency equation for cross-isobaric absolute vorticity ζ_a is

$$\frac{\partial \zeta_a}{\partial t} = -(\mathbf{V}_H - \mathbf{V}_C) \cdot \nabla_p \zeta_a - \omega \frac{\partial \zeta_a}{\partial p} - \zeta_a D - \left(\frac{\partial \omega}{\partial x} \frac{\partial v}{\partial p} - \frac{\partial \omega}{\partial y} \frac{\partial u}{\partial p} \right) \quad (1)$$

where \mathbf{V}_H and ∇_p are as defined in Sect. 3.2, $\mathbf{V}_C \equiv (u_C, v_C)$ is the cyclone velocity estimated from the cyclone track in Fig. 10l, ω is the vertical velocity in pressure coordinate, and D is the isobaric divergence. The right hand side of (1) comprises (from left to right) the following forcing terms: (1) horizontal advection (HADV), (2) vertical advection (VADV), (3) stretching of vertical vortex tubes (STRC), and (4) tilting of horizontal vortex tubes (TILT). The cyclone velocity only affects horizontal advection and hence the time tendency in the co-moving.

Figure 12a–e show that HADV and VADV contribute negatively to the cyclone development. On the other hand, terms of STRC and TILT are positive. In particular, STRC is more dominant and is mainly responsible for spinning up the cyclone. The net forcing shows maximum positive tendency west of the absolute vorticity maximum and the cyclone centre, as horizontal convergence maximizes there leading to strong vertical vortex stretching. As a result, the cyclone migrates westward with time.

While the sign of each term is roughly the same in the mature stage (Fig. 12f–j) as in the developing stage, the magnitude of every term, especially STRC, is much larger. Additionally, positive tendency is seen in the HADV and VADV denoting that advection is bringing high-vorticity air to the cyclone centre from the northwest and from lower levels where the vorticity generation is stronger. TILT shows a north-south dipole structure resulting from the maximum rising motion located at the centre of the dipole under ambient easterly wind shear. The net positive forcing still lies west of the absolute vorticity maximum and the cyclone centre as that is where vertical vortex stretching is the strongest, but negative tendency is also found in the southwestern and southern sector of the cyclone due to the tilting effect.

Higher up in the atmosphere (600 hPa) in the mature stage (Fig. 12k–o), HADV, VADV and STRC are largely opposite to those at 850 hPa: absolute vorticity is advected

Borneo vortex and meso-scale convective rainfall

S. Koseki et al.

Title Page	
Abstract	Introduction
Conclusions	References
Tables	Figures
◀	▶
◀	▶
Back	Close
Full Screen / Esc	
Printer-friendly Version	
Interactive Discussion	



Borneo vortex and meso-scale convective rainfall

S. Koseki et al.

Title Page

Abstract

Introduction

Conclusions

References

Tables

Figures

◀

▶

◀

▶

Back

Close

Full Screen / Esc

Printer-friendly Version

Interactive Discussion



upward and westward from the lower levels while horizontal divergence is destroying the vorticity. TILT still has a dipole structure, but in the east-west rather than north-south direction. The net forcing is still positive west of the vorticity maximum and the cyclone centre mainly due to vertical advection from the lower levels. At even higher levels (~250 hPa, not shown), while the tendency of each forcing term is similar to those at 600 hPa, the net forcing is only weakly positive.

In summary, vortex stretching mainly occurs at low levels and the ambient cross-isobaric absolute vorticity is rapidly intensified and advected to the mid-troposphere where it is destroyed by isobaric divergence. This is the primary reason for the spin-up and sustenance of a meso- α cyclone with the shallow vertical structure. The tilting of vortex tubes generates both positive and negative cross-isobaric absolute vorticity and this serves only to re-organize the vorticity distribution on the isobaric surface in the mature stage.

6.2 What maintains the strong convergence in the meso- α cyclone?

While low-level vortex stretching due to isobaric convergence is mainly responsible for the intensification of the cyclone, what process is responsible for the maintenance of the convergence around the cyclone centre?

Appendix B shows that the divergence tendency equation in the frame co-moving with the cyclone centre can be written as

$$\frac{\partial D}{\partial t} = -2(\mathbf{V}_H - \mathbf{V}_C) \cdot \nabla_p D + \nabla_p \cdot \left\{ -\frac{\partial}{\partial p} [\omega (\mathbf{V}_H - \mathbf{V}_C)] \right\} - \frac{3}{2} D^2 - 2\lambda^2 + \frac{1}{2} \zeta_a^2 - \nabla_p^2 \Phi - \beta(u - u_c), \quad (2)$$

where λ is the deviatoric strain (deformation less the effect of the horizontal divergence) rate of the isobaric flow field and β is the gradient of the Coriolis parameter. The other symbols are as defined in Sect. 6.1. The right hand side of Eq. (2) comprises seven forcing terms: twice the horizontal advection of divergence (HADD), divergence of the horizontal stress due to vertical transport of momentum (VMOM), self-enhancement of convergence or self-inhibition of divergence (SELF), destruction by deviatoric strain

(STRN), generation by centrifugal acceleration due to local rotation (CENT), divergence of the pressure-gradient force denoted by the Laplacian of pressure field (LAP), and beta-effect on zonal wind. The beta-effect was found to be much weaker than the other terms and will not be shown here.

Figure 13 shows the horizontal distribution of first six forcing terms in Eq. (2) at 850 hPa in the mature stage. The beta-effect is much weaker than the other terms and is not shown. CENT and LAP are very strong but have similar distributions of opposite signs (Fig. 13a and b). They represent a basic balance between the outward centrifugal and inward pressure-gradient forces in a cyclone, although some residual local divergent tendency is seen (Fig. 13c) which explains the net divergent tendency (Fig. 13h). An approximate balance is also seen between HADD and VMOM (Fig. 13d and e). This means the convergence and divergence generated by horizontal stress northwest of the vortex centre (Fig. 13e) are mostly removed by (twice) the advection from the northeasterly wind (Fig. 13d). The dipole structure of VMOM has its origin as follows: at low levels, upward flow maximises near $(x, y) = (-30 \text{ km}, 10 \text{ km})$ where the wind is northeasterly; this creates a local maximum in southwesterly stress (since the horizontal momentum is lost to mid-levels) and leads to stress convergence upwind and stress divergence downwind. The net convergence tendency (Fig. 13h) is due mainly to SELF (Fig. 13g). However, the self-enhancement of convergence relies on the existence of net convergence in the first place. We suggest that deviatoric strain provides the original seed for the convergence tendency in the cyclone because STRN is the only negative-definite forcing in Eq. (2) and it is strongest where SELF and the net convergence tendency are the strongest (cf. Fig. 13f, g and h).

The net convergence and net divergence tendencies appear to be evenly matched in Fig. 13h, consistent with the weak net growth of the cyclone in the mature stage. In the developing stage, although each term is weaker than in the mature stage, their distributions are approximately the same and the net forcing of convergence is stronger than that of divergence, resulting that the overall growth of convergence in the cyclone (not shown). Therefore, we suggest the Borneo vortex is spun-up primarily by

Borneo vortex and meso-scale convective rainfall

S. Koseki et al.

Title Page

Abstract

Introduction

Conclusions

References

Tables

Figures

◀

▶

◀

▶

Back

Close

Full Screen / Esc

Printer-friendly Version

Interactive Discussion



the low-level convergence (Sect. 6.1) which is originally forced by the deviatoric strain associated with the northeasterly surge turning northwesterly upon crossing the equator (e.g. around 107° E in Fig. 8b and c). The subsequent growth and maintenance of vortex is mainly by the self-enhancement effect of convergence.

5 **6.3 How is the comma-shaped rainband organized in the meso- α cyclone?**

The northern and northeastern sweep of the comma-shaped rainband away from the cyclone centre was already noted (Fig. 10). Here, we examine the reason for such departure from axisymmetry.

10 The most intense convergence is located near the cyclone centre (Fig. 14a) and but strong convergence is also seen in the northern and northeastern sectors consistent with the location of the comma-shaped rainband (Fig. 10b). Conversely, a divergence zone is seen in the southern and eastern sectors adjacent to the cyclone centre. The zonal ($\partial u/\partial x$) and meridional ($\partial v/\partial y$) contributions to divergence (Figs. 14b and c) both show quadrupole structure within ~ 150 km from the cyclone centre. 15 Beyond ~ 150 km, the zonal and meridional convergence patches are stronger in the northwestern and northeastern sectors, respectively.

In a typical snapshot of the meso- α cyclone in the mature stage (Fig. 14d), finer structures in the form of three or four rainfall patches 10–100 km in size can be seen along the comma tail of the rainband. In the northeastern sector, the confluence of 20 oppositely directed meridional winds is mainly responsible for the meso- β scale convergence and rainfall evidenced by the co-location of the zero meridional wind line and the comma-tail of the rainband. In fact, the intensities of the convergence and rainfall in the comma-tail are comparable with those in the comma-head. This fact is not apparent in the temporal mean picture (Figs. 10b and 14a) because the zero meridional wind 25 line is not stationary relative to the cyclone centre (Fig. 14e). Once formed, advection by the cyclonic and radially converging wind system would bring the meso- β scale rain cells into the northwestern sector and the comma-head. In other words, the meso- α

Borneo vortex and meso-scale convective rainfall

S. Koseki et al.

Title Page

Abstract

Introduction

Conclusions

References

Tables

Figures

◀

▶

◀

▶

Back

Close

Full Screen / Esc

Printer-friendly Version

Interactive Discussion



scale organization of the northeasterly surge and southeasterly cyclonic wind in the northeastern sector is the root cause of the rainband's departure from axisymmetry.

Figure 15 analyses the dynamic and thermodynamic profiles across the meridional confluence line in the mature stage. Below 800 hPa, the confluence of southerly and northerly winds is evident (Fig. 15a). Below 850 hPa, higher (lower) equivalent potential temperature θ_e associated with warmer and more humid (cooler and drier) conditions is found south (north) of the confluence line (Fig. 15b). In fact, the frontal nature of the confluence line is clearly marked by a narrow zone of sharp θ_e -gradient. This is largely consistent with the southerly (northerly) origin of the air mass in the equatorial South China Sea (continental Asia). The narrow ridge of θ_e (Fig. 15b) near the zero meridional wind line (Fig. 15a) is due to warm air and water vapour being transported upward by the intense rising motion (Fig. 15a) arising from the low-level meridional convergence. In fact, the θ_e -ridge and ω -trough reaches into the middle- and upper-troposphere representing a curtain of warm, moist conveyor turrets in the northeastern sector of the Borneo vortex which plays an analogous role in transport to the warm conveyor belts of extra-tropical cyclones.

With reference to Fig. 15c, 70–80% of the total rainfall at the confluence front is contributed by the cloud microphysics scheme in the model. The peak rainfall from the cumulus parameterization is less pronounced at the confluence front. However, cumulus parameterization is the main contributor to the secondary maximum in rainfall around 60–70 km south of the front. Much less rainfall occurs north of the front. So, to a large extent, the strong upward motion due to the low-level frontal confluence induces condensation and rain formation which in turn releases latent heat that has a positive feedback on the rising motion. Such a mechanism of rain formation is similar to that in the Meiyu-Baiu front over the western North Pacific Ocean (e.g., Moteki et al., 2004a, b), although the spatio-temporal scale and the underlying frontal dynamics are very different.

As the rainfall along the confluence front exhibits a strong diurnal cycle (similar to that depicted in Fig. 9b), the role of convection in frontal rain formation cannot be neglected.

Borneo vortex and meso-scale convective rainfall

S. Koseki et al.

Title Page	
Abstract	Introduction
Conclusions	References
Tables	Figures
◀	▶
◀	▶
Back	Close
Full Screen / Esc	
Printer-friendly Version	
Interactive Discussion	



**Borneo vortex and
meso-scale
convective rainfall**

S. Koseki et al.

Title Page

Abstract

Introduction

Conclusions

References

Tables

Figures

◀

▶

◀

▶

Back

Close

Full Screen / Esc

Printer-friendly Version

Interactive Discussion



With reference to Fig. 15d, the convective available potential energy (CAPE) has two peaks: one higher at the front and the other lower around -60 – 70 south of the front. Relatedly, the level of neutral buoyancy (LNB) is highest at the front and there is another peak around 60 – 70 km south of the front. CAPE and LNB are larger south of the front than north of it. This difference is attributed to the higher equivalent potential temperature of the near surface air in the south (Fig. 15b). The lifting condensation level (LCL) has a minimum at the front and is consistently lower south of the front than north of it. Thus, larger CAPE and LNB indicate stronger conditional instability south of the front while lower LCL there allows the conditional instability to be more readily released by rising air. In other words, CAPE, LNB and LCL work together to encourage cumulus convection and rainfall south of the front. Since the highest CAPE and LNB and lowest LCL found at the front, the strongest convection and heaviest rainfall would also occur at the front.

Now, what maintains the meso- β scale convergence and hence the rainband at the confluence front? The divergence tendency diagnostic in Eq. (2) for the confluence front is shown in Fig. 16. CENT is not significant implying that local rotation is not an important dynamical factor at the meso- β scale (Fig. 16a). The contribution of LAP is relatively weak and its distribution is similar to that of the much stronger VMOM (Figs. 16b and d). The latter is because of the alignment between the pressure-gradient force and the horizontal stress. An approximate balance between HADD (Fig. 16c) and (VMOM+LAP) holds at the meso- β scale. Along the confluence front, the net convergence tendency (Fig. 16g) comes mainly from SELF (Fig. 16f). But again, the negative-definite STRN which maximizes along the front (Fig. 16e) is likely to be the origin of the convergence tendency. Therefore, the convergence along the confluence front (Fig. 16h) is forced originally by the deviatoric strain inherent in the confluence of the northeasterly surge and the southwesterly cyclonic wind in the Borneo vortex, and this is subsequently intensified by nonlinear self-enhancement dynamics.

7 Concluding remarks

We have investigated the Borneo vortex and meso-scale convective rainband associated with the monsoon cold surge over the equatorial South China Sea.

The composite analysis based on Cold Surge Index revealed that the strong cold surge transports absolute vorticity and water vapour from the higher tropical latitudes to the equatorial region. The daily rainfall over the South China Sea is enhanced significantly when the strong cold surge occurs and its distribution matches roughly with vorticity and water vapour flux convergence in the lower troposphere. The diurnal cycle of rainfall showed that rainfall over the South China Sea is intensified over the whole day, whereas rainfall over the Java Sea is reinforced only in night-morning time. This is consistent with the fact that the rainfall over the Java Sea is mainly due to the interaction of the seaward land breeze and the landward monsoon wind whereas the rainfall over the equatorial South China Sea is organized by larger-scale dynamics. Other composite analyses of the Borneo vortex show intense rainfall and convergence in the north and northeast sectors of the Borneo vortex but shed little light on mesoscale structure or processes.

The semi-idealized experiment using NHM has shown well-organized features of the Borneo vortex and the comma-shaped rainband over the equatorial South China Sea associated with cold surge. Diagnostics of absolute vorticity tendency revealed that vortex stretching due to intense low-level convergence is mostly responsible for growth of the cyclone. The divergence tendency budget analysis suggested that the strong convergence around the meso- α cyclone core is caused by the deviatoric strain and maintained by self-enhancement.

A comma-shaped rainband is seen sweeping north and northeast from the centre of the meso- α cyclone with clusters of meso- β scale rainfall patches. The cyclonic south-easterly flow (warm and wet) collides with the northeasterly surge (cool and dry) in the northeastern sector of the meso- α cyclone. The frontal confluence generates strong rising motion which is associated with much condensation and rain formation. Thermo-

Borneo vortex and meso-scale convective rainfall

S. Koseki et al.

Title Page

Abstract

Introduction

Conclusions

References

Tables

Figures

◀

▶

◀

▶

Back

Close

Full Screen / Esc

Printer-friendly Version

Interactive Discussion



dynamic factors such as convective available potential energy and lifting condensation level show consistency with enhanced convective propensity at the confluence front. The divergence tendency budget analysis along the confluence front indicate once more that the deviatoric strain inherent in the confluent wind field spawns the convergence at the confluence front and self-enhancement dynamics greatly intensifies the convergence maintaining the rainband.

Our results in this paper reveal new detailed features of the meso- β scale structure of the Borneo vortex in the organization of the comma-shaped rainband. The dynamical mechanisms for growth and maintenance of the vortex and the confluence front are also clarified.

As a possible future investigation, mesoscale observations of Borneo vortices would help to elucidate how realistic our simulation results are. Moreover, because the resolution of our experiment is only 10 km, we have not explored the meso- γ scale (1–10 km) dynamics in the convective towers of the rainband in the Borneo vortex. Advanced numerical experiment with finer resolution would seem desirable.

Appendix A

Definition of the centre of the meso- α cyclone

The centre of the Borneo vortex and meso- α cyclone in sections 4 and 5 is defined in this section. First, the mean low-level wind $(U_{i,j}, V_{i,j})$ over a centred 3×3 -point moving grid is defined as

$$U_{i,j} = \frac{1}{9} \sum_{k=-1}^1 \sum_{l=-1}^1 (u_{i+k,j+l}), V_{i,j} = \frac{1}{9} \sum_{k=-1}^1 \sum_{l=-1}^1 (v_{i+k,j+l}). \quad (\text{A1})$$

where $u_{i,j}$, and $v_{i,j}$ are average zonal and meridional winds from 800 to 950 hPa. Here, i and j are the zonal and meridional indices of a grid point, respectively. The magnitude

Borneo vortex and meso-scale convective rainfall

S. Koseki et al.

Title Page

Abstract

Introduction

Conclusions

References

Tables

Figures

◀

▶

◀

▶

Back

Close

Full Screen / Esc

Printer-friendly Version

Interactive Discussion



of the mean wind is thus,

$$U_{i,j} = \sqrt{U_{i,j}^2 + V_{i,j}^2}. \quad (\text{A2})$$

We define the location of the minimum $U_{i,j}$ in the cyclone as the cyclone centre at every hour, because the cyclonic flow in the immediate neighbourhood of the centre nearly cancels out, leaving sometimes a weak background wind.

Appendix B

Deviation of the tendency equations for absolute vorticity and divergence

The horizontal momentum equations in the frame co-moving with the cyclone centre are

$$\frac{\partial u}{\partial t} + (u - u_c) \frac{\partial u}{\partial x} + (v - v_c) \frac{\partial u}{\partial y} + \omega \frac{\partial u}{\partial p} = f(v - v_c) + \Omega_z^2 \Delta x - \frac{\partial \Phi}{\partial x} - A_x, \quad (\text{B1})$$

$$\frac{\partial v}{\partial t} + (u - u_c) \frac{\partial v}{\partial x} + (v - v_c) \frac{\partial v}{\partial y} + \omega \frac{\partial v}{\partial p} = -f(u - u_c) + \Omega_z^2 \Delta y - \frac{\partial \Phi}{\partial y} - A_y, \quad (\text{B2})$$

where for convenience, beta-plane dynamics is assumed. Cartesian coordinates $(x, y) \equiv (x_0 + \Delta x, y_0 + \Delta y)$ such that $\Delta x \ll x_0, \Delta y \ll y_0$ represent displacements in the east-west and north-south directions respectively. u and v are zonal and meridional winds respectively; $\omega \equiv Dp/Dt$ is the cross-isobaric velocity in p -coordinate where p denotes pressure. Φ is the geopotential. $f \equiv f(y_0) + \beta \Delta y$ is the latitude-dependent Coriolis parameter, where f_0 and β take the constant values characteristic of the reference latitude at y_0 . $(\Omega_z^2 \Delta x, \Omega_z^2 \Delta y)$ is the f plane representation of the centrifugal acceleration, where $\Omega_z \equiv \frac{1}{2} f(y_0)$ is the Earth's rotation rate of in the local vertical direction at y_0 . (The beta-plane representation of centrifugal acceleration is not necessary or consistent here as $O(\Delta x^2, \Delta x \Delta y, \Delta y^2)$ terms are neglected.) $\mathbf{V}_C \equiv (u_c, v_c)$ and $\mathbf{A}_C \equiv (A_x, A_y)$

are the velocity and acceleration in the motion of the cyclone center in Fig. 10l and so are functions of time t only.

Taking the difference of the isobaric derivatives, $\partial(B1)/\partial y$ minus $\partial(B2)/\partial x$, gives

$$\frac{\partial \zeta}{\partial t} = -(\mathbf{V}_H - \mathbf{V}_C) \cdot \nabla_p \zeta - \omega \frac{\partial \zeta}{\partial p} - \zeta D - \left(\frac{\partial \omega}{\partial x} \frac{\partial v}{\partial p} - \frac{\partial \omega}{\partial y} \frac{\partial u}{\partial p} \right) - fD - \beta(v - v_c)$$

- 5 where $\zeta \equiv v_x - u_y$ is the relative vorticity on an isobaric surface. Thus, the tendency equation for absolute vorticity on an isobaric surface $\zeta_a \equiv f + \zeta$ can be derived as in Eq. (1).

Taking the sum of the isobaric derivatives $\partial(B1)/\partial x$ and $\partial(B2)/\partial y$ gives

$$\frac{\partial D}{\partial t} = -(\mathbf{V}_H - \mathbf{V}_C) \cdot \nabla_p D - \omega \frac{\partial D}{\partial p} - \nabla_p \omega \cdot \frac{\partial(\mathbf{V}_H - \mathbf{V}_C)}{\partial p} - D^2 + 2J(u, v) + f\zeta + \frac{1}{2}f^2 - \nabla_p^2 \Phi - \beta(u - u_c), \quad (B3)$$

- 10 where $D \equiv \partial u / \partial x + \partial v / \partial y$ is the isobaric divergence and $J(u, v) \equiv u_x v_y - v_x u_y$ is the Jacobian of the horizontal wind. Now, the Jacobian can be rewritten as

$$J(u, v) = \frac{1}{4} (D^2 + \zeta^2) - \lambda^2. \quad (B4)$$

where λ is the deviatoric horizontal strain rate, i.e. λ and $-\lambda$ are eigenvalues of the deviatoric strain tensor S :

$$15 \quad S \equiv \begin{pmatrix} a & b \\ b & -a \end{pmatrix}$$

where $a \equiv \frac{1}{2}(u_x - v_y)$, $b \equiv \frac{1}{2}(v_x + u_y)$. S measures the deformation of the flow field less the effect of horizontal divergence. Moreover, by the continuity equation, $-\partial \omega / \partial p = D$, the second and third terms on the right hand side of (B3) can be rewritten as

$$\begin{aligned} -\omega \frac{\partial D}{\partial p} - \nabla_p \omega \cdot \frac{\partial(\mathbf{V}_H - \mathbf{V}_C)}{\partial p} &= -\omega \frac{\partial D}{\partial p} + \omega \nabla_p \cdot \frac{\partial(\mathbf{V}_H - \mathbf{V}_C)}{\partial p} - \nabla_p \cdot \left[\omega \frac{\partial(\mathbf{V}_H - \mathbf{V}_C)}{\partial p} \right] \\ 20 \quad &= \nabla_p \cdot \left\{ -\frac{\partial}{\partial p} [\omega(\mathbf{V}_H - \mathbf{V}_C)] \right\} - (\mathbf{V}_H - \mathbf{V}_C) \cdot \nabla_p D - D^2. \end{aligned} \quad (B5)$$

Borneo vortex and meso-scale convective rainfall

S. Koseki et al.

Title Page	
Abstract	Introduction
Conclusions	References
Tables	Figures
◀	▶
◀	▶
Back	Close
Full Screen / Esc	
Printer-friendly Version	
Interactive Discussion	



Combining Eqs. (B4) and (B5) and using $\zeta_a \equiv f + \zeta$, the tendency equation for horizontal divergence can be derived as in Eq. (2).

Acknowledgements. The authors are grateful to K. Saito and S. Hayashi of Meteorological Research Institute, Japan Meteorological Agency, M. Sawada of Tohoku University, M. Inatsu of Hokkaido University, for their advice in running NHM. The authors would also like to express appreciation to K. K. W. Cheung of Macquarie University and S. Otsuka of Kyoto University for meaningful discussions about the Borneo vortex. This work comprises in part Earth Observations of Singapore contribution XX.

References

- 10 Asai, T.: Meso-scale features of heavy snowfalls in Japan Sea coastal region of Japan, *Tenki*, 35, 156–161, 1988 (in Japanese).
- Braesicke, P., Ooi, S. H., and Samah, A. A.: Properties of strong off-shore Borneo vortices: a composite analysis of flow pattern and composition as captured by ERA-Interim, *Atmos. Sci. Lett.*, 13, 128–132, doi:10.1002/asl.372, 2012.
- 15 Chambers, C. R. S. and Li, T.: Simulation of formation of a near-equatorial typhoon Vamei (2001), *Meteorol. Atmos. Phys.*, 98, 67–80, doi:10.1007/s00703-006-0229-0, 2007.
- Chang, C.-P., Liu, C.-H., and Kuo, H.-C.: Typhoon Vamei: An equatorial tropical cyclone Formation, *Geophys. Res. Lett.*, 30, 1150, doi:10.1029/2002GL016365, 2003.
- 20 Chang, C.-P., Harr, P. A., and H.-J. Chen, H.-J.: Synoptic disturbances over the equatorial South China Sea and western Maritime Continent during boreal winter, *Mon. Weather Rev.*, 133, 489–503, doi:10.1175/MWR-2868.1, 2005.
- Chen, G. T. J., Gerish, T. E., and Chang, C.-P.: Structure variations of the synoptic-scale cyclonic disturbances near Borneo during WMONEX period, *Pap. Meteorol. Res.*, 9, 117–135, 1986.
- 25 Chen, J. M., Chang, C.-P., and Li, T.: Annual cycle of the South China sea surface temperature using the NCEP/NCAR reanalysis, *J. Meteorol. Soc. Jpn.*, 81, 879–884, doi:10.2151/jmsj.81.879, 2003.
- Chen, T.-C., Tsay, J.-D. Yen, M.-C. and Matsumoto, J.: Interannual variation of the late fall in central Vietnam, *J. Climate*, 25, 392–213, doi:10.1175/JCLI-D-11-00068.1, 2012.

Borneo vortex and meso-scale convective rainfall

S. Koseki et al.

Title Page

Abstract

Introduction

Conclusions

References

Tables

Figures

◀

▶

◀

▶

Back

Close

Full Screen / Esc

Printer-friendly Version

Interactive Discussion



- Estoque, M. A.: The sea breeze as a function of the prevailing synoptic situation, *J. Atmos. Sci.*, 19, 244–250, doi:10.1175/1520-0469(1962)019i0244:TSBAAF;2.0.CO;2, 1962.
- Frank, W. M.: The structure and energetics of the tropical cyclone I: Storm structure, *Mon. Weather Rev.*, 105, 1119–1135, doi:10.1175/1520-0493(1977)105i1119:TSAEOT;2.0.CO;2, 1977.
- Hadi T. W., Horinouchi, T., Tsuda, T., Hashiguchi, H., and Fukao, S.: Sea-breeze circulation over Jakarta, Indonesia: A climatology based on boundary layer radar observations, *Mon. Weather Rev.*, 130, 2153–2166, doi:10.1175/1520-0493(2002)130i2153:SBCOJI;2.0.CO;2, 2002.
- Hattori, M., Mori, S., and Matsumoto, J.: The Cross-Equatorial Northerly Surge over the Maritime Continent and Its Relationship to Precipitation Patterns, *J. Meteorol. Soc. Jpn.*, 89A, 27–47, doi:10.2151/jmsj.2011-A02, 2011.
- Hayashi, S., Aranami, K., and Saito, K.: Statistical Verification of Short Term NWP by NHM and WRF-ARW with 20km Horizontal Resolution around Japan and Southeast Asia. *SOLA*, 4, 133–136, doi:10.2151/sola.2008-034, 2008.
- Holland, G. J. and Merrill, R. T.: On the dynamics of tropical cyclone structural-changes, *Q. J. Roy. Meteor. Soc.*, 110, 723–745, doi:10.1002/qj.49711046510, 1984.
- Hong, C.-C., Hsu, H.-H., and Chia, H.-H.: A Study of East Asian Cold Surges during the 2004/05 Winter: Impact of East Asian Jet Stream and Subtropical Upper-Level Rossby Wave Trains, *Terr. Atmos. Ocean. Sci.*, 20, 333–343, doi:10.3319/TAO.2008.02.04.01(A), 2009.
- Hubert, L. F., Kruger, A. F., and Winston, J. S.: Double Intertropical Convergence Zone- Fact and Fiction?, *J. Atmos. Sci.*, 26, 771–773, doi:10.1175/1520-0469(1969)026i0771:TDICZF;2.0.CO;2, 1969.
- Huffman, G. J., Adler, R. F., Bolvin, D. T., Gu, G. J., Nelkin, E. J., Bowman, K. P., Hong, Y., Stocker, E. F., and Wolff, D. B.: The TRMM multisatellite precipitation analysis (TMPA): Quasi-global, multiyear, combined-sensor precipitation estimates at fine scales, *J. Hydrometeorol.*, 8, 38–55, doi:10.1175/JHM560.1, 2007.
- Ikawa, M. and Saito, K.: Description of a non-hydrostatic model developed at the Forecast Research Department of the MRI, *MRI Tech. Rep.* 28, 238 pp., 1991.
- Johnson, R. H. and Houze Jr., R. A.: Precipitating cloud systems of the Asian monsoon. *Monsoon Meteorology*, edited by: Chang, C.-P. and Krishnamurti, T. N., Oxford University Press, 298–353, 1987.

Borneo vortex and meso-scale convective rainfall

S. Koseki et al.

Title Page

Abstract

Introduction

Conclusions

References

Tables

Figures

◀

▶

◀

▶

Back

Close

Full Screen / Esc

Printer-friendly Version

Interactive Discussion



Joseph B., Bhatt, B. C., Koh, T.-Y. and Chen. S.: Sea breeze simulation over the Malay Peninsula in an intermonsoon period, *J. Geophys. Res.*, 113, D20122, doi:10.1029/2008JD010319, 2008.

Joung, C. H. and Hitchman, M. H.: On the role of successive downstream development in East Asian polar air outbreaks, *Mon. Weather Rev.*, 110, 1224–1237, doi:10.1175/1520-0493(1982)110;1224:OTROSD;2.0.CO;2, 1982.

Juneng, L. and Tangang, F. T.: Long-term trends of winter monsoon synoptic circulations over the maritime continent: 1962–2007, *Atmos. Sci. Lett.*, 11, 199–203, doi:10.1002/asl.272, 2010.

Kain, J. S.: The Kain-Fritsch convective parameterization: An update. *J. Appl. Meteorol.*, 43, 170–181, doi:10.1175/1520-0450(2004)043;0170:TKCPAU;2.0.CO;2, 2004.

Kawashima M. and Fujiyoshi, Y.: Shear instability wave along a snowband: Instability structure, evolution, and energetic derived from dual-Doppler radar data, *J. Atmos. Sci.*, 62, 351–370, doi:10.1175/JAS-3392.1, 2005.

Koseki, S., Koh, T.-Y., and Teo, C.-K.: Effects of the cold tongue in the South China Sea on the monsoon, diurnal cycle and rainfall in the Maritime Continent, *Q. J. Roy. Meteor. Soc.*, early online published, doi:10.1002/qj.2052, 2013.

Kumagai, Y.: Improvement of the land surface processes in JMANHM, CAS/JSC WGNE Res, *Activ. Atmos. Oceanic Modell.*, 34, 0419–0420, 2004a.

Lau, K.-M. and Chang C.-P.: Planetary scale aspects of winter monsoon and Teleconnections, *Monsoon Meteorology*, edited by: Chang, C.-P. and Krishnamurti, T. N., Oxford University Press, 161–202, 1987

Lim, H. and Chang, C.-P.: A Theory of Mid-latitude Forcing of Tropical Motions during Winter Monsoon, *J. Atmos. Sci.*, 38, 2377–2392, doi:10.1175/1520-0469(1981)038;2377:ATFMFO;2.0.CO;2, 1981.

Lu, M.-M. and Chang, C.-P.: Unusual Late-Season Asian Cold Surges during the 2005 Asian Winter Monsoon: Roles of Atlantic Blocking and the Central Asian Anticyclone, *J. Climate*, 22, 5205–5217, doi:10.1175/2009JCLI2935.1, 2009.

Mak, M. K. and Walsh, J. E.: On the Relative Intensities of Sea and Land Breezes, *J. Atmos. Sci.*, 33, 242–251, doi:10.1175/1520-0469(1976)033;0242:OTRIOS;2.0.CO;2, 1976.

Moteki, Q, Uyeda, H., Maesaka, T., Shinoda, T., Yoshizaki, M., and Kato, T.: Structure and development of two merged rainbands observed over the East China Sea during X-BAIU-99

Borneo vortex and meso-scale convective rainfall

S. Koseki et al.

Title Page

Abstract

Introduction

Conclusions

References

Tables

Figures

◀

▶

◀

▶

Back

Close

Full Screen / Esc

Printer-friendly Version

Interactive Discussion

part I : Meso-beta-scale structure and development processes, *J. Meteorol. Soc. Jpn.*, 82, 19–44, doi:10.2151/jmsj.82.19, 2004a.

Moteki, Q, Uyeda, H., Maesaka, T., Shinoda, T., Yoshizaki, M., and Kato, T.: Structure and development of two merged rainbands observed over the East China Sea during X-BAIU-99 part II : Meso-alpha-scale structure and build-up processes of convergence in the Baiu frontal region, *J. Meteorol. Soc. Jpn.*, 82, 45–65, doi:10.2151/jmsj.82.45, 2004b.

Nagata, M.: On the structure of a convergent cloud band over the Japan Sea in winter: A prediction experiment, *J. Meteorol. Soc. Jpn.*, 65, 871–883, 1987.

Nagata, M.: Meso-beta-scale vortices developing along the Japan-Sea polar-airmass convergence zone (JPCZ) cloud band: Numerical simulation, *J. Meteorol. Soc. Jpn.*, 71, 43–57, 1993.

Nakanishi, M.: Improvement of the Mellor-Yamada turbulence closure model based on large-eddy simulation data, *Bound-Lay. Meteorol.*, 99, 349–378, doi:10.1023/A:1018915827400, 2001.

Nakanishi, M. and Niino, H.: An improved Mellor-Yamada level-3 model with condensation physics: Its design and verification, *Bound-Lay. Meteorol.*, 112, 1–31, doi:10.1023/B:BOUN.0000020164.04146.98, 2004.

Nakanishi, M. and Niino, H.: An improved Mellor-Yamada level-3 model: Its numerical stability and application to a regional prediction of advection fog, *Bound-Lay Meteorol.*, 119, 397–407, doi:10.1007/s10546-005-9030-8, 2006.

Onogi, K., Tsitstui, J., Koide, H., Sakamoto, M., Kobayashi, S., Hatsushika, H., Matsumoto, T., Yamazaki, N., Kamahori, H., Takahashi, K., Kadokura, S., Wada, K., Kato, K., Oyama, R., Ose, T., Mannoji, N., and Taira, R.: The JRA-25 Reanalysis, *J. Meteorol. Soc. Jpn.*, 85, 369–432, doi:10.2151/jmsj.85.369, 2007.

Qian J. H., Robertson, A. W., and Moron, V.: Interactions among ENSO, the Monsoon, and Diurnal Cycle in Rainfall Variability over Java, Indonesia, *J. Atmos. Sci.*, 67, 3509–3524, doi:10.1175/2010JAS3348.1, 2010.

Saito, K., Fujita, T., Yamada, Y., Ishida, J. I., Kumagai, Y., Aranami, K., Ohmori, S., Nagasawa, R., Kumagai, S., Muroi, C., Kato, T., Eito, H., and Yamazaki, Y.: The operational JMA nonhydrostatic mesoscale model, *Mon. Weather Rev.*, 134, 1266–1298, doi:10.1175/MWR3120.1, 2006.

Borneo vortex and meso-scale convective rainfall

S. Koseki et al.

Title Page

Abstract

Introduction

Conclusions

References

Tables

Figures

◀

▶

◀

▶

Back

Close

Full Screen / Esc

Printer-friendly Version

Interactive Discussion



Saito, K., Ishida, J. I., Aranami, K., Hara, T., Segawa, T., Narita, M., and Honda, Y.: Nonhydrostatic atmospheric models and operational development at JMA, *J. Meteorol. Soc. Jpn.*, 85B, 271–304, doi:10.2151/jmsj.85B.271, 2007.

Seko, H., Hayashi, S., Kunii, M., and Saito, K.: Structure of the Regional Heavy Rainfall System that Occurred in Mumbai, India, 26 July 2005, *SOLA*, 4, 129–132, doi:10.2151/sola.2008-033, 2008.

Takaya, K. and Nakamura, H.: Mechanisms of intraseasonal amplification of the cold Siberian high, *J. Atmos. Sci.*, 62, 4423–4440, doi:10.1175/JAS3629.1, 2005.

Tangang, F. T., Juneng, L., Salimun, E., Vinayachandran, P. N., Seng, Y. K., Reason, C. J. C., Behera, S. K., and Yasunari, T.: On the roles of the northeast cold surge, the Borneo vortex, the Madden-Julian Oscillation, and the Indian Ocean Dipole during the extreme 2006/2007 flood in southern Peninsular Malaysia, *Geophys. Res. Lett.*, 35, L14S07, doi:10.1029/2008GL033429, 2008.

Tomita, T. and Yasunari, T.: Role of the northeast winter monsoon on the biennial oscillation of the ENSO/monsoon system, *J. Meteorol. Soc. Jpn.*, 74, 399–413, 1996.

Trilaksono, N. J., Otsuka, S., and Yoden, S.: A Time-Lagged Ensemble Simulation on the Modulation of Precipitation over West Java in January–February 2007, *Mon. Weather Rev.*, 140, 601–616, doi:10.1175/MWR-D-11-00094.1, 2012.

Tsuboki, K. and Asai, T.: The multi-scale structure and development mechanism of mesoscale cyclones over the sea of Japan in winter, *J. Meteorol. Soc. Jpn.*, 82, 597–621, doi:10.2151/jmsj.2004.597, 2004.

Wangwongchai, A., Zhao, S. X., and Zeng, Q. C.: A case study on a strong tropical disturbance and record heavy rainfall in Hat Yai, Thailand during the winter monsoon, *Adv. Atmos. Sci.*, 22, 436–450, doi:10.1007/BF02918757, 2005.

**Borneo vortex and
meso-scale
convective rainfall**

S. Koseki et al.

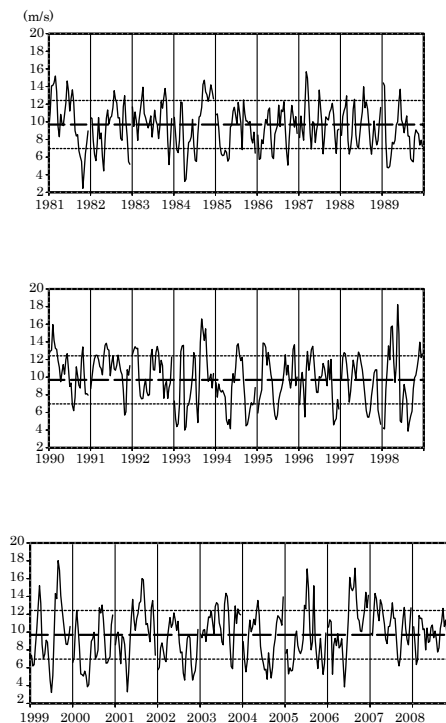


Fig. 1. Cold Surge (CS) Index obtained from daily JRA25/JCDAS in December from 1981 to 2008. Thick dashed line is the climatology of CS Index and thin dot lines are the climatology \pm one standard deviation of CS Index. CS Index is defined as area-averaged wind speed at 850 hPa over 7.5° N to 12.5° N and 110° E to 115° E. The vertical lines in plots demarcate the time series for each year emphasizing that the plot are not continuous multiyear time series.

[Title Page](#)[Abstract](#)[Introduction](#)[Conclusions](#)[References](#)[Tables](#)[Figures](#)[◀](#)[▶](#)[◀](#)[▶](#)[Back](#)[Close](#)[Full Screen / Esc](#)[Printer-friendly Version](#)[Interactive Discussion](#)

Borneo vortex and meso-scale convective rainfall

S. Koseki et al.

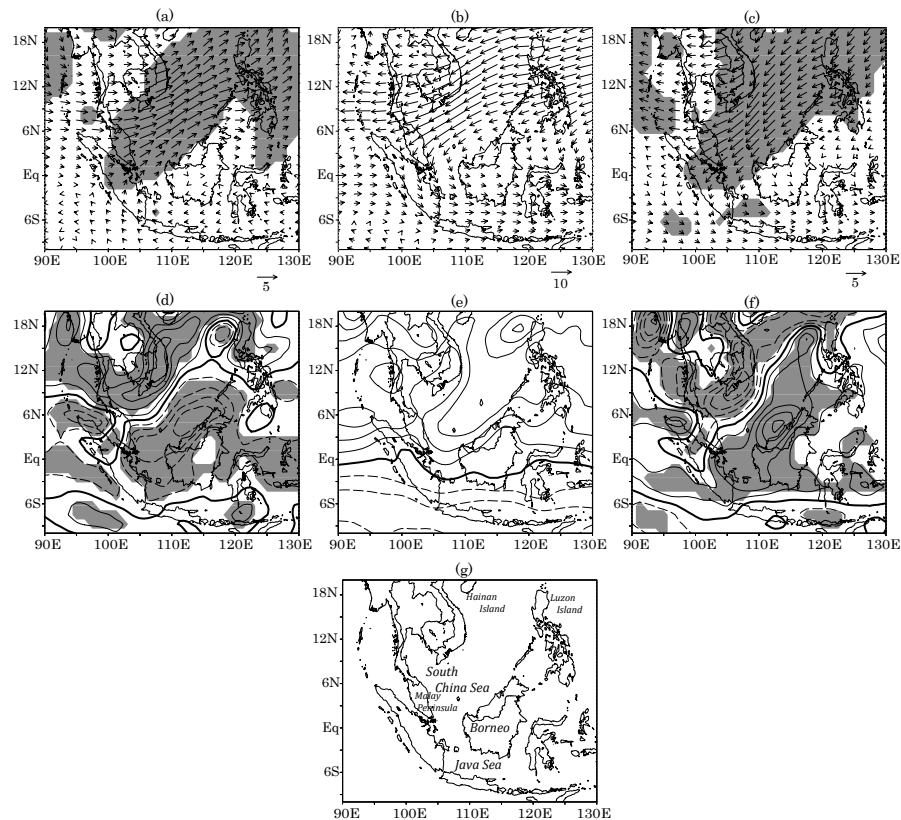


Fig. 2. JRA25/JCDAS data for **(b)** and **(e)** climatology of horizontal wind (vector) and absolute vorticity at 850 hPa in December, **(a)** and **(c)** difference in horizontal wind during NS and SS composite from the climatology at 850 hPa, and **(d)** and **(f)** difference in absolute vorticity during NS and SS composite from the climatology at 850 hPa. Thick black contour denotes zero value. Positive (negative) value is represented as solid (dashed) line in **(d–f)**. Gray shade is significant level of 95 %. Contour interval is $1.0 \times 10^{-4} \text{ s}^{-1}$ for **(e)** and $0.2 \times 10^{-4} \text{ s}^{-1}$ for **(d)** and **(f)**.

[Title Page](#)
[Abstract](#)
[Introduction](#)
[Conclusions](#)
[References](#)
[Tables](#)
[Figures](#)
[Back](#)
[Close](#)
[Full Screen / Esc](#)
[Printer-friendly Version](#)
[Interactive Discussion](#)

Borneo vortex and
meso-scale
convective rainfall

S. Koseki et al.

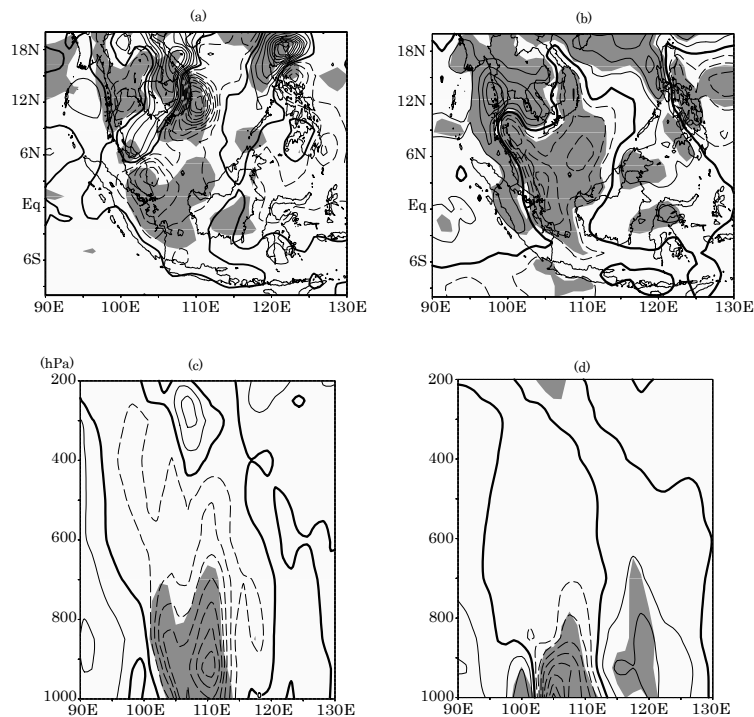


Fig. 3. (a–b) Divergence of absolute vorticity and water vapour fluxes anomalies during SS obtained from JRA25/JCDAS at 850 hPa in December. **(c)** and **(d)** Pressure-longitude sections of **(a)** and **(b)** respectively averaged between 0° and 4° N. Black solid (dashed) line is positive (negative) value. Contour interval is $5 \times 10^{-5} \text{ s}^{-1} \text{ day}^{-1}$ for **(a)**, $0.2 \times 10^{-1} \text{ g kg}^{-1} \text{ day}^{-1}$ for **(b)**, $0.2 \times 10^{-5} \text{ s}^{-1} \text{ day}^{-1}$ for **(c)**, and $0.1 \times 10^{-1} \text{ g kg}^{-1} \text{ day}^{-1}$ for **(d)**. Thick black contour denotes the value of zero. Gray shade is significant level of 95% for the difference from the climatology.

Title Page

Abstract

Introduction

Conclusions

References

Tables

Figures

◀

▶

◀

▶

Back

Close

Full Screen / Esc

Printer-friendly Version

Interactive Discussion



**Borneo vortex and
meso-scale
convective rainfall**

S. Koseki et al.

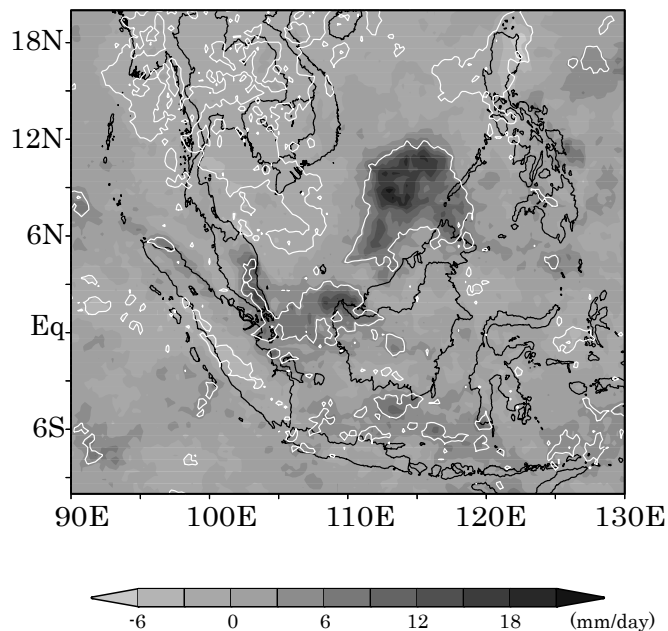


Fig. 4. Daily rainfall anomalies during SS obtained from TRMM version 3B42. White contour is significant level of 90% for the difference from the climatology.

Title Page

Abstract

Introduction

Conclusions

References

Tables

Figures

◀

▶

◀

▶

Back

Close

Full Screen / Esc

Printer-friendly Version

Interactive Discussion



Borneo vortex and meso-scale convective rainfall

S. Koseki et al.

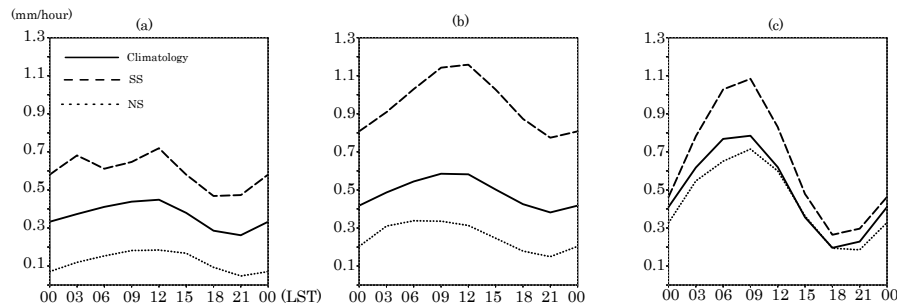


Fig. 5. 3 hourly rainfall averaged over **(a)** equatorial South China Sea ($0\text{--}4^\circ\text{ N}$ and $105\text{--}109^\circ\text{ E}$), **(b)** South China Sea north of Borneo ($7\text{--}12^\circ\text{ N}$ and $111\text{--}116^\circ\text{ E}$), and **(c)** Java Sea ($6\text{--}3^\circ\text{ S}$ and $106\text{--}115^\circ\text{ E}$) during NS (long-short dashed line), climatology (solid line), and SS (dashed line).

[Title Page](#)
[Abstract](#)
[Introduction](#)
[Conclusions](#)
[References](#)
[Tables](#)
[Figures](#)
[◀](#)
[▶](#)
[◀](#)
[▶](#)
[Back](#)
[Close](#)
[Full Screen / Esc](#)
[Printer-friendly Version](#)
[Interactive Discussion](#)


Borneo vortex and meso-scale convective rainfall

S. Koseki et al.

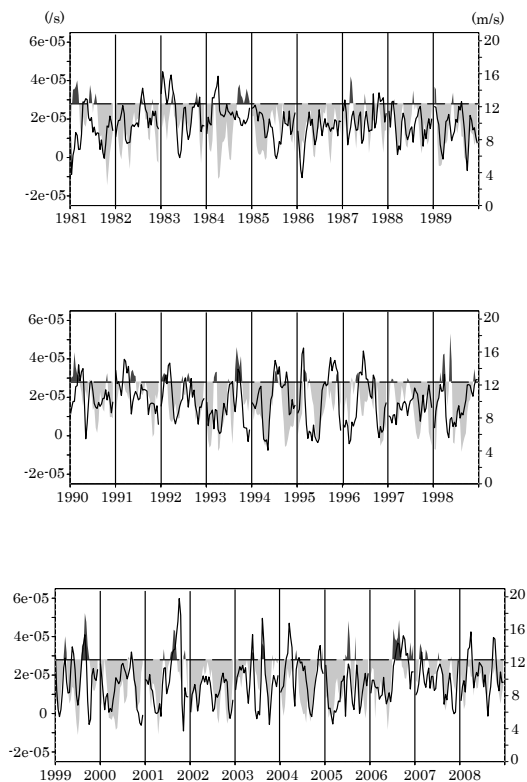


Fig. 6. Temporal sequences of daily CS Index (shade) and Marine the Borneo vortex (MBV) Index (line) in December obtained from JRA25/JCDAS. Dark (light) shade is CS Index larger (smaller) than climatology plus one standard deviation of CS Index. Dashed line denotes the climatology plus one standard deviation of MBV Index. The vertical lines in plots demarcate the time series for each year emphasizing that the plot are not continuous multiyear time series.

Title Page

Abstract

Introduction

Conclusions

References

Tables

Figures

◀

▶

◀

▶

Back

Close

Full Screen / Esc

Printer-friendly Version

Interactive Discussion



Borneo vortex and
meso-scale
convective rainfall

S. Koseki et al.

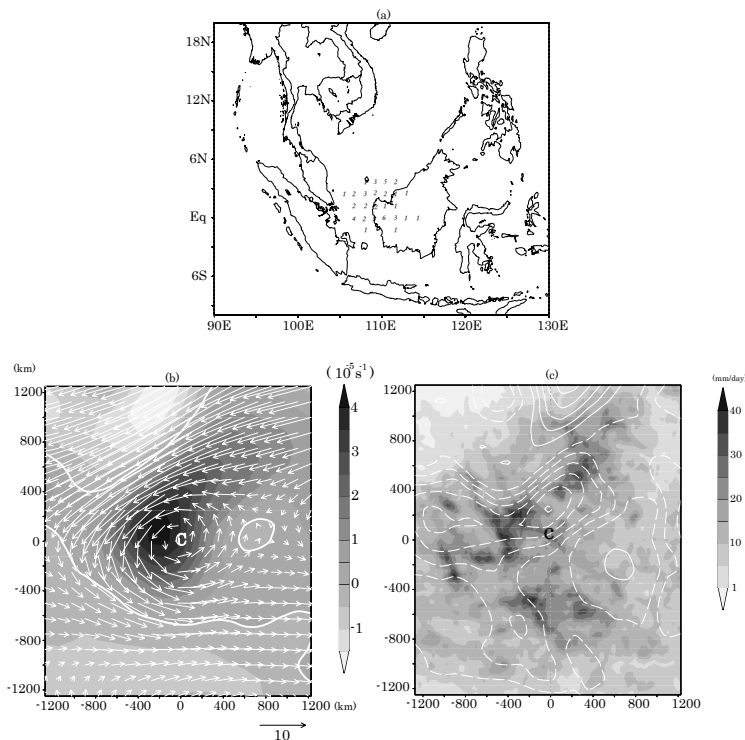


Fig. 7. (a) Location of Borneo vortex centre obtained from JRA25/JCDAS. The number of each grid counts the number of day when the centre is located at each grid. (b) Composite of absolute vorticity (shaded) and horizontal wind (vector) at 850 hPa from JRA25/JCDAS around the centre of Borneo vortex. White thick contour denotes the value of zero of absolute vorticity. (c) Composite of horizontal divergence (contour, interval is 10^{-6} s^{-1}) at 850 hPa from JRA25/JCDAS and hourly rainfall (shaded) from TRMM around the centre of the Borneo vortex. Solid (dashed) line means positive (negative) value. C denotes the centre of composite Borneo vortex.

Borneo vortex and
meso-scale
convective rainfall

S. Koseki et al.

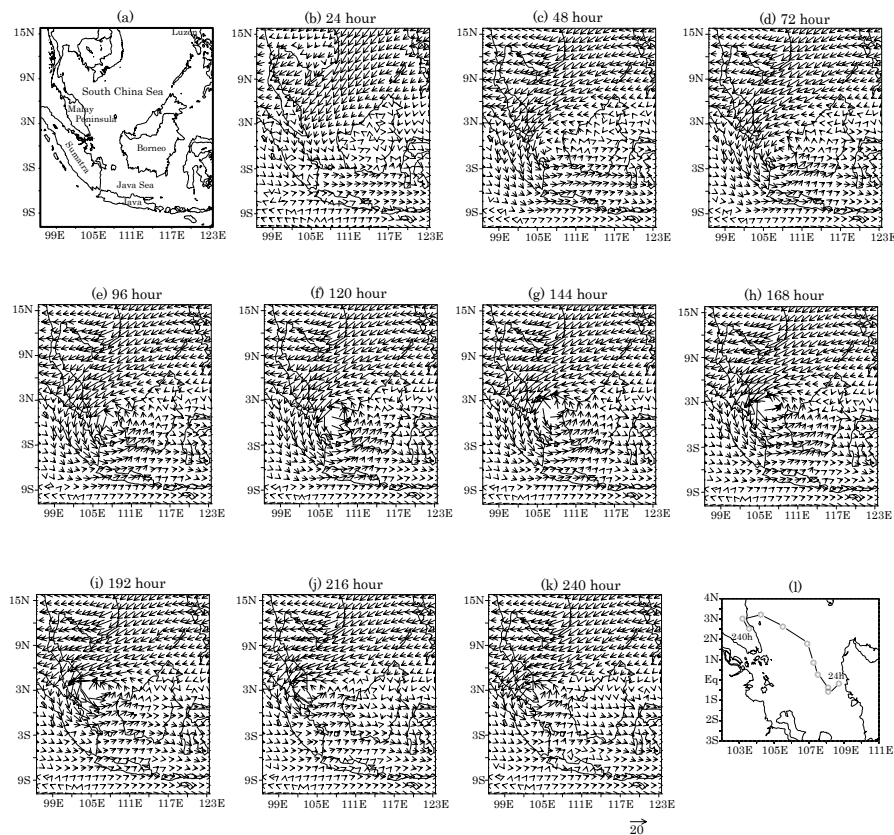


Fig. 8. (a) Domain of the semi-idealized experiment. (b–k) 24 hourly temporal evolution in simulated Borneo vortex from 24 to 240 hours from initialization. (l) shows the 24-hourly cyclone track.

**Borneo vortex and
meso-scale
convective rainfall**

S. Koseki et al.

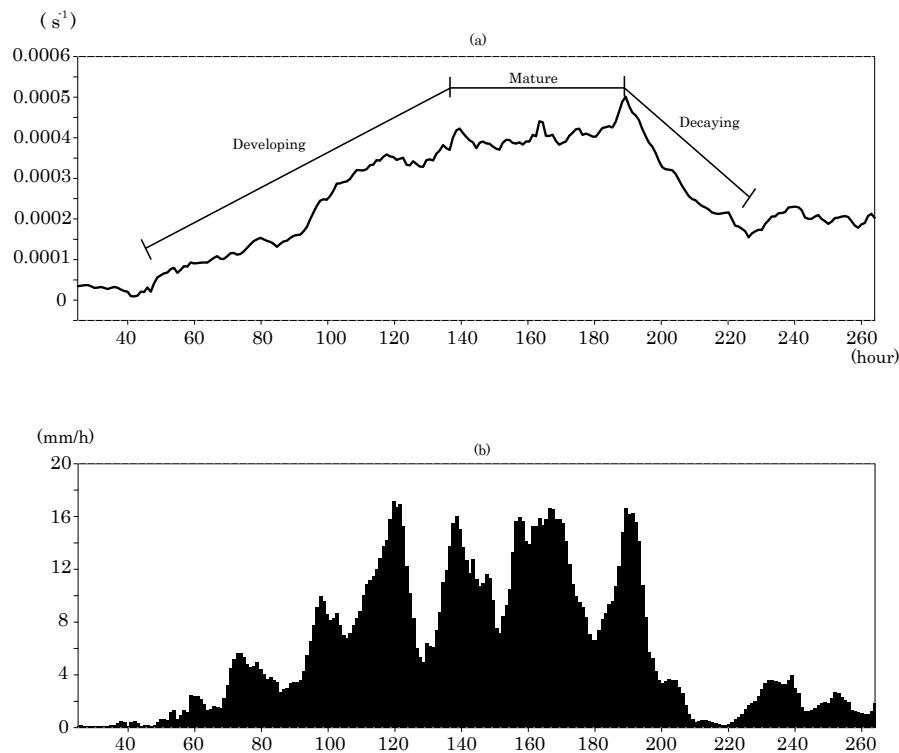


Fig. 9. Time sequences of (a) absolute vorticity at 850 hPa and (b) hourly rainfall averaged within a radius of 200 km of the centre of simulated meso- α cyclone.

**Borneo vortex and
meso-scale
convective rainfall**

S. Koseki et al.

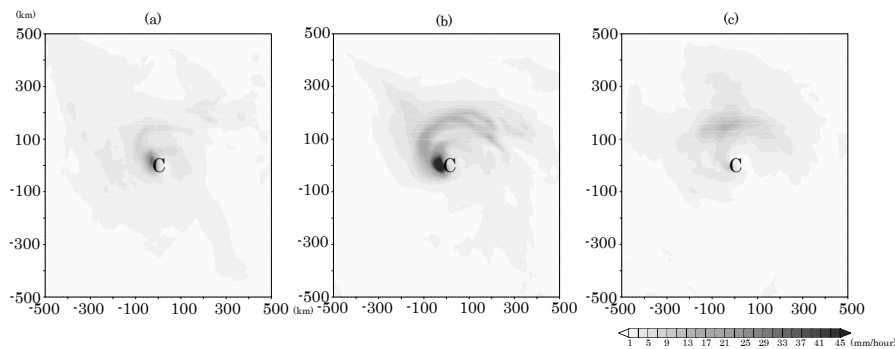


Fig. 10. Temporal mean of hourly rainfall around the centre of simulated meso- α cyclone in the (a) developing stage, (b) mature stage, and (c) decaying stage. C denotes the centres of composite meso- α cyclone.

Title Page

Abstract

Introduction

Conclusions

References

Tables

Figures

◀

▶

◀

▶

Back

Close

Full Screen / Esc

Printer-friendly Version

Interactive Discussion



Borneo vortex and meso-scale convective rainfall

S. Koseki et al.

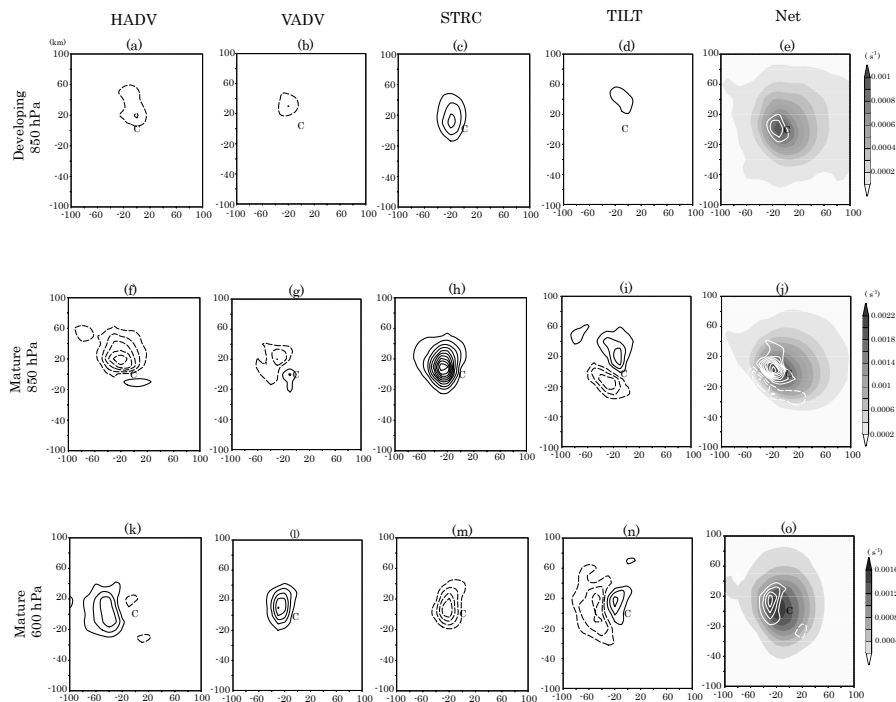


Fig. 12. Temporal mean of **(a)** HADV, **(b)** VADV, **(c)** STRC, **(d)** TILT and **(e)** net forcing in Eq. (1) in the developing stage at 850 hPa. Solid (dashed) lines denote positive (negative) values. The contour interval is 10^{-6} s^{-2} . **(f–j)** and **(k–o)** are same as for **(a–e)**, but for the mature stage at 850 hPa and 600 hPa, respectively. The shading shows absolute vorticity. C denotes the centre of meso- α cyclone.

Borneo vortex and
meso-scale
convective rainfall

S. Koseki et al.

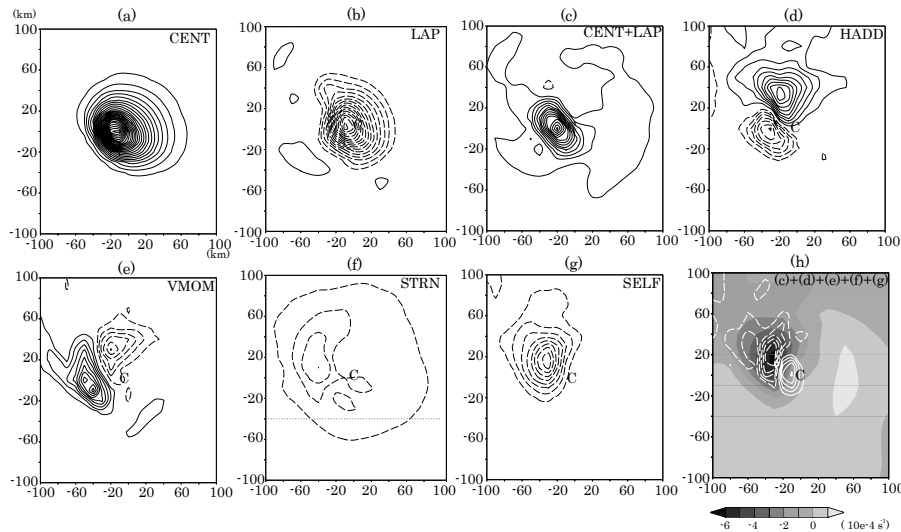


Fig. 13. Temporal mean of **(a)** CENT, **(b)** LAP, **(c)** HADD, **(d)** VMOM, **(e)** CENT+LAP, **(f)** SHADD+VMOM, **(g)** STRN, **(h)** SELF and **(i)** net forcing of divergence in the Eq. (2) in the mature stage at 850 hPa. Solid (dashed) lines denote positive (negative) values. The contour interval is 10^{-6} s^{-2} . The shading shows divergence. C denotes the centre of meso- α cyclone.

Borneo vortex and
meso-scale
convective rainfall

S. Koseki et al.

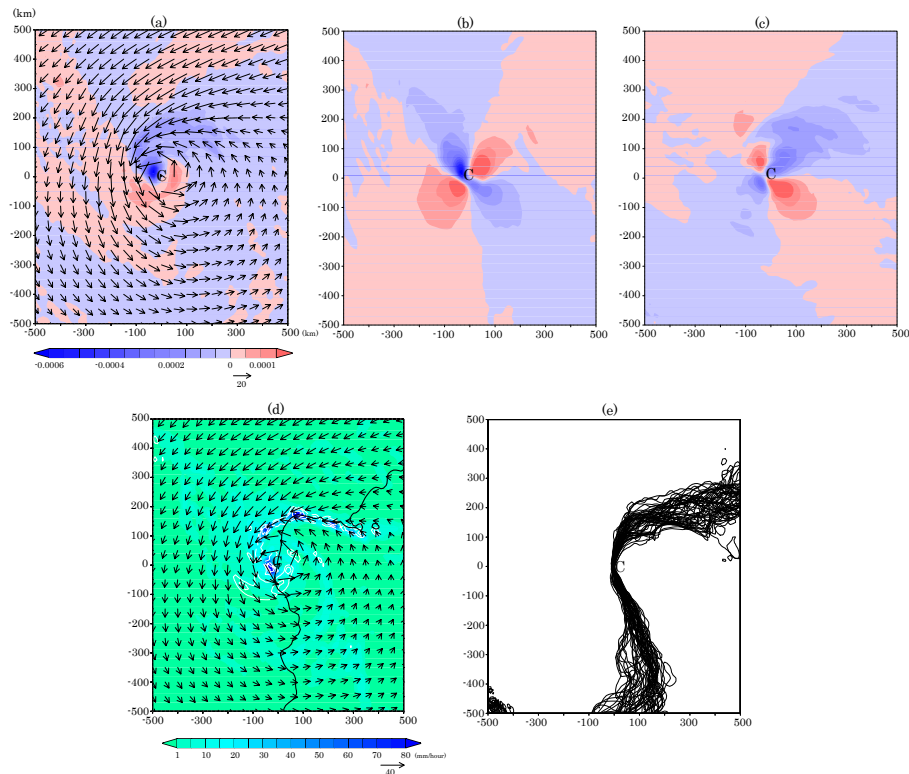


Fig. 14. (a) Temporal mean of horizontal divergence (shade) and horizontal wind (vector) in the mature stage at 850 hPa. This horizontal convergence is decomposed into (b) zonal and (c) meridional components. (d) Snapshot of horizontal divergence (white contours), hourly rainfall (shade), and horizontal wind (vector), and the zero meridional wind line (black contour) at 850 hPa at 140 h after the initialization. The white contours have intervals of 0.0002 s^{-1} . Solid (dashed) lines denote positive (negative) values. (e) Zero meridional lines plotted at hourly intervals in the mature stage. C denotes the centre of meso- α cyclone.

Borneo vortex and
meso-scale
convective rainfall

S. Koseki et al.

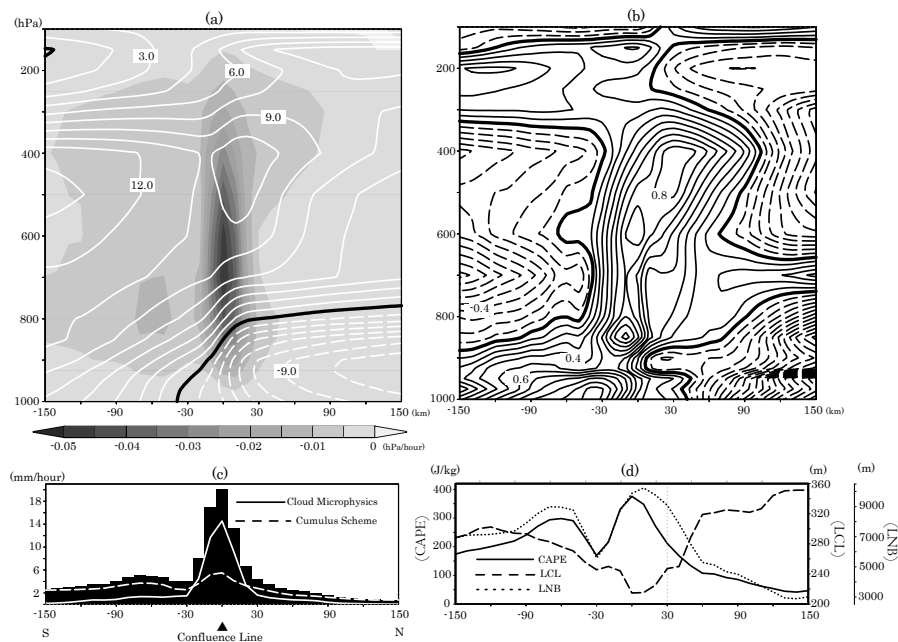


Fig. 15. Meridional sections of **(a)** vertical velocity, ω (shade) and meridional wind (contour), **(b)** deviation of equivalent potential temperature from its meridional mean (taken within 150 km of the confluence line), **(c)** hourly rainfall and the contributions from the cloud microphysics and cumulus schemes, and **(d)** convective available potential energy (CAPE, left scale), lifting condensation level (LCL, right inner scale), and neutral buoyancy level (NBL, right outer scale). All sections are taken across and averaged along the confluence lines in Fig. 14e for x between 100 and 300 km in the mature stage and then temporally averaged. The contour intervals are 1.5 m s^{-1} in **(a)** and 0.1 K in **(b)** and solid (dashed) lines denote positive (negative) values. Zero contours in **(a)** and **(b)** are marked as thick black lines. Positive (negative) displacement in the abscissa refers to distance north (south) of the confluence line at all times.

Title Page

Abstract

Introduction

Conclusions

References

Tables

Figures

◀

▶

◀

▶

Back

Close

Full Screen / Esc

Printer-friendly Version

Interactive Discussion

Borneo vortex and
meso-scale
convective rainfall

S. Koseki et al.

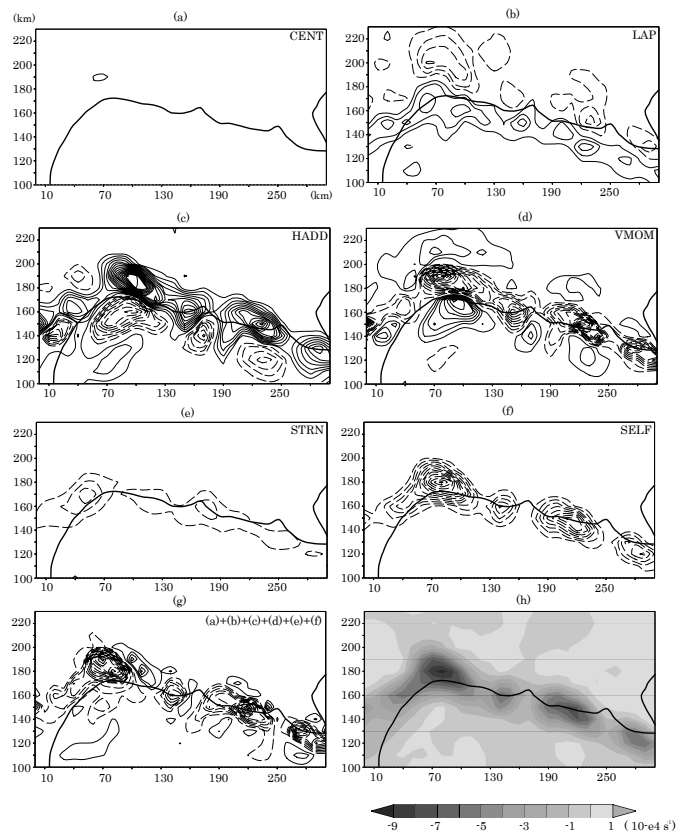


Fig. 16. Snapshot of the divergence tendency budget (cf. Eq. 2) along the meridional confluence front in northeastern part of the meso- α cyclone for **(a)** CENT, **(b)** LAP, **(c)** HADD, **(d)** VMOM, **(e)** STRN, **(f)** SELF, and **(g)** net forcing at 850 hPa at 140 h after the initialization. **(h)** is divergence at same level and time. The contouring convention is the same as in Fig. 13. The thick black contour is the zero meridional wind line.

Title Page

Abstract

Introduction

Conclusions

References

Tables

Figures

◀

▶

◀

▶

Back

Close

Full Screen / Esc

Printer-friendly Version

Interactive Discussion

